An integrated multiangle, multispectral, and polarimetric imaging concept for aerosol remote sensing from space

David J. Diner[a], Russell A. Chipman[b], Neil Beaudry[b], Brian Cairns[c], Leslie D. Foo[d], Steven A. Macenka[a], Thomas J. Cunningham[a], Suresh Seshadri[a], and Christoph Keller[e]
[a]Jet Propulsion Laboratory, Caltech, 4800 Oak Grove Drive, Pasadena, CA, 91109
[b]University of Arizona, Tucson, AZ, 85721
[c]Columbia University, New York City, NY, 10025
[d]Optical Research Associates, Tucson, AZ, 85711
[e]National Solar Observatory, Tucson, AZ, 85719

ABSTRACT

Techniques for passive remote sensing of aerosol optical and microphysical properties from space include visible, near- and shortwave-infrared imaging (e.g., from MODIS), multiangle intensity imaging (e.g., ATSR-2, AATSR, MISR), near-ultraviolet mapping (e.g., TOMS/OMI), and polarimetry (e.g., POLDER, APS). Each of these methods has unique strengths. In this paper, we present a concept for integrating these approaches into a unified sensor. Design goals include spectral coverage from the near-UV to the shortwave infrared; intensity and polarimetric imaging simultaneously at multiple view angles; global coverage within a few days; kilometer to sub-kilometer spatial resolution; and measurement of the degree of linear polarization (DOLP) for a subset of the spectral complement with an uncertainty of 0.5% or less. This high polarimetric accuracy is the most challenging aspect of the design, and is specified in order to achieve climate-quality uncertainties in optical depth, refractive index, and other microphysical properties. Based upon MISR heritage, a pushbroom multi-camera architecture is envisioned, using separate line arrays to collect imagery within each camera in the different spectral bands and in different polarization orientations. For the polarimetric data, accurate cross-calibration of the individual line arrays is essential. An electro-optic polarization "scrambler", activated periodically during calibration sequences, is proposed as a means of providing this cross-calibration. The enabling component is a rapid retardance modulator. Candidate technologies include liquid crystals, rotating waveplates, and photoelastic modulators (PEMs). The PEM, which uses a piezoelectric transducer to induce rapid time-varying stress birefringence in a glass bar, appears to be the most suitable approach. An alternative measurement approach, also making use of a PEM, involves synchronous demodulation of the oscillating signal to reconstruct the polarization state. The latter method is potentially more accurate, but requires a significantly more complex detector architecture.

1. INTRODUCTION

Providing an accurate description of aerosol distributions and microphysical properties is essential for evaluating and validating aerosol transport and climate models. Such models are essential for understanding the underlying causes of climate change and environmental impacts. However, since many aerosol parameters, such as optical depth, single-scattering albedo, particle size distribution, particle shape, refractive index, and vertical distribution jointly govern top-of-atmosphere radiances, retrievals from space are generally underconstrained. The effects of the underlying surface and clouds add to this complexity.

A number of remote sensing techniques have been used for satellite aerosol retrievals, and each has unique strengths. Multispectral intensity techniques, e.g., from the Moderate resolution Imaging Spectroradiometer (MODIS), provide sensitivity to particle size along with column optical depth using spectral bands ranging from the visible to the shortwave infrared[1,2]. Near-ultraviolet mapping from the Total Ozone Mapping Spectrometer (TOMS)[3] (and with the recent launch of the Aura satellite, the Ozone Monitoring Instrument, OMI[4]) offers a unique approach in that most surfaces are dark at these wavelengths, and the interaction between aerosol and Rayleigh scattering provides sensitivity to aerosol absorption. Multiangle intensity data provide constraints on particle size and sphericity along with optical depth by virtue of sampling the particle scattering phase function[5,6]. Over many aerosol source regions, e.g., desert and urban areas, where the ground reflectance is high, multiangle intensity imaging, e.g., from the Multi-angle Imaging SpectroRadiometer (MISR) and from

the Along-Track Scanning Radiometer (ATSR) successors, takes advantage of differences in the spatial and angular reflectance signatures of the surface and atmosphere to retrieve aerosol properties over many surface types[7-11]. At the sub-kilometer spatial resolution provided by MISR, automated pattern matching algorithms enable stereoscopic retrieval of cloud-top and plume-top heights with vertical precision of 500 m and accuracy of about 500-1000 m[12-15].

Polarimetry can provide data exceeding the capabilities of intensity measurements alone by providing sensitivity to size-resolved refractive index (hence constraining composition), improving accuracy in optical depth, single-scattering albedo, and providing tighter constraints on particle size distributions. The utility of multiangle polarimetric data, acquired at visible and shortwave infrared wavelengths, has been demonstrated through sensitivity studies[16], airborne measurements using the Research Scanning Polarimeter (RSP)[17-19], and with the spaceborne Polarization and Directionality of Earth's Reflectances (POLDER)[20] instrument. The POLDER design has polarimetric uncertainty of ~2%[21]. The Aerosol Polarimeter Sensor (APS) planned for the National Polar-orbiting Operational Environmental Satellite System (NPOESS) will extend spectral coverage into the shortwave infrared (SWIR) and improve linear polarization uncertainty to ~0.2%. However, APS is non-imaging, limited to a single along-track scan one pixel wide.

Since each of the aforementioned measurement techniques has a unique set of strengths, fusing their capabilities into an integrated sensor is a powerful way of reducing indeterminacy and improving measurement accuracy. We envision an integrated sensor that combines the salient features of many instruments into a single instrument, as shown in Table 1. The benefits of an integrated sensor include: (1) improved retrieval accuracies due to a greater range of constraints on aerosol particle properties, (2) simultaneity of measurements, which is important due to the high variability of aerosols in time and space, (3) moderately high resolution to deal with cloud discrimination and cross-track coverage to include surface validation sites within the field of view, and (4) cost savings by building one instrument instead of many. Of the measurement requirements listed as design goals, the most challenging is achieving 0.5% uncertainty in degree of linear polarization (DOLP), particularly for an imager. This requirement results from the recommendations of climate workshops[21,23], which seek accuracies of 0.01 - 0.02 in optical depth and ~0.03 in single scattering albedo, i.e., about a factor of 2-3 better than the current state-of-the art. Figure 1 shows the results of simulations, indicating that with a multiangle intensity-only instrument having nine angles (as with MISR) but broader spectral coverage, these goals are not quite achieved. Increasing the number of angles provides little benefit. Incorporation of polarization provides significant improvement, but only if the uncertainty in DOLP is limited to 0.5% or better. DOLP uncertainty of 2% is not sufficient to improve sensitivity relative to what can be achieved with multiangle intensity radiometry, though there is a gain in sensitivity to refractive index.

Table 1: Aerosol sensor characteristics

	Spatial resolution	Along-track angle range	Spectral range	Polarization accuracy	Global coverage
MISR	275 m - 1.1 km	70° fore - 70° aft	446 - 866 nm	NA	9 days
MODIS	250 m - 1 km	NA	469 - 2130 nm	NA	2 days
ATSR-2/AATSR	1 - 2 km	0°, 55° fore	550 - 1610 nm	NA	5 days
POLDER	6 - 7 km	60° fore - 60° aft	443 - 910 nm	~2%	2 days
APS	6 - 20 km	60° fore - 60° aft	412 - 2250 nm	0.2%	No
TOMS/OMI	20 - 40 km	NA	270 - 500 nm	NA	1 day
Concept	250 m - 2 km	70° fore - 70° aft	380 - 2130 nm	0.5%	3 - 4 days

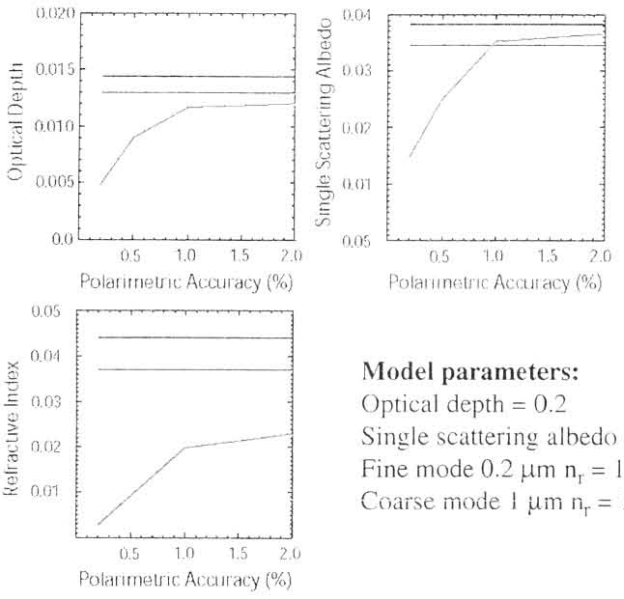

Figure 1. Sensitivity to optical depth, single scattering albedo, and real part of the refractive index as a function of accuracy in measurement of *DOLP*.

Model parameters:
Optical depth = 0.2
Single scattering albedo = 0.9
Fine mode 0.2 μm n_r = 1.45
Coarse mode 1 μm n_r = 1.35

intensity only (9 angles), intensity only (17 angles), intensity + polarization (9 angles)

2. INSTRUMENT ARCHITECTURE

The starting point for our instrument design concept is the MISR instrument aboard NASA's Terra satellite[24], which flies in sun-synchronous polar orbit at an altitude of 705 km. MISR observes the Earth at nine different view zenith angles in four spectral bands (446, 558, 672, 866 nm), using a separate pushbroom camera at each angle. This strategy permits the focal lengths to change with angle in order to preserve ground resolution. The fore-aft cameras acquire images with view angles, relative to the Earth's surface, at 0°, 26°, 46°, 60°, and 70°. In its global observing mode, the data in all bands of the nadir camera, and the red band data of all of the off-nadir cameras are downlinked at full spatial resolution, 275 m. All other channels are averaged on-board to 1.1-km resolution. For the integrated sensor, we have selected 380, 412, 446, 558, 672, 866, 1375, 1630, and 2130 as the nominal wavelengths bands. The spectral bands selected for polarization measurements are 672 and 1630 nm (see Fig. 2). The rationale for these choices is based upon the instrument heritage described above, and to achieve refractive index sensitivity for both accumulation and coarse mode aerosols.

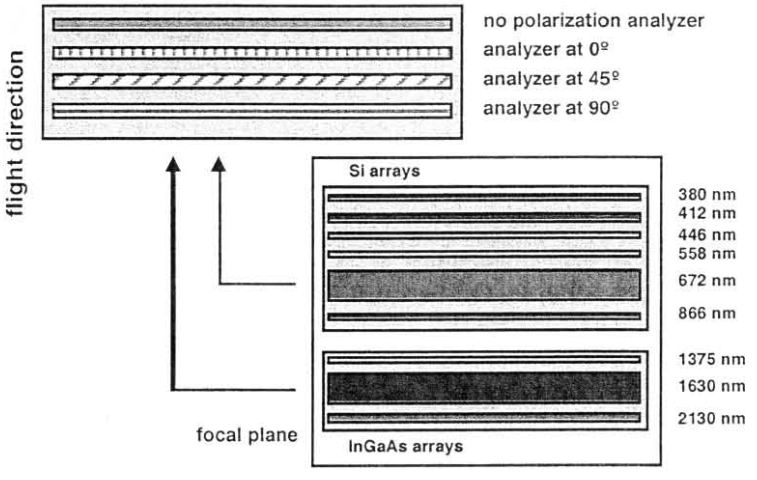

Figure 2. Conceptual focal plane layout for the integrated sensor. Like MISR, each camera would contain a focal plane containing linear arrays, so that imagery is acquired in pushbroom fashion. However, a greater number of spectral bands is envisioned, and in two bands (one visible and one shortwave infrared), polarization measurements would be acquired. The detector material is Si for the wavelengths shortward of 1 μm, and InGaAs for the remainder.

To reduce the global coverage time relative to MISR (9 days), we investigated a range of sun-synchronous orbit altitudes. We find that an orbit at 640 km, for example, can achieve 4-day global coverage with a swath width less than twice that of MISR (725 km vs. 380 km). It is possible to achieve 3-day or even 2-day coverage by increasing the orbit altitude, but maintaining ground resolution (in order to provide adequate cloud screening) would require a commensurate increase in camera focal length. From 640 km altitude, 250 m pixels require a 32 mm lens, assuming 12.5 μm detector pitch. The requisite swath can be achieved with a cross-track field of view of ±29°, requiring 2900 pixels in each line array. As with MISR, on-board averaging of certain channels is envisioned to reduce the downlink data rate.

MISR uses refractive lenses containing 7 glass elements in a telecentric design. To acquire intensity images that are insensitive to polarization, Lyot depolarizers are placed in front of the cameras. Clearly, this approach cannot be used for a next-generation instrument that needs to acquire both intensity and polarization measurements from each camera. The broader spectral coverage also implies then need for a reflective, rather than refractive, design. We find that a three-element reflector can in principle meet the necessary design requirements, using a combination of silver and aluminum coatings to achieve high reflectivity at each surface.

In MISR, multispectral data are acquired from each camera by placing filter stripes above each of the line arrays in the camera focal planes[24]. For those bands where polarimetry is desired in the next-generation sensor, the spectral filters over different line arrays would be supplemented with analyzers in different orientations, manufactured from a material such as Corning Polarcor (a glass substrate embedded with silver microneedles) or other high extinction polarizing material (see Fig. 2). In such a pushbroom system the different line arrays pass over the same point within a short time interval. MISR experience shows that the data can be digitally superimposed after the fact to better than 1/10 of a pixel. To achieve even finer co-registration, which is essential for accurate polarimetry, the high resolution data would be co-registered, then summed to a resolution of 1 or 2 km. MISR experience also shows that cross-calibration uncertainty between channels of 1-2% is possible only after extensive effort. Thus, because the proposed method uses separate line arrays to reconstruct the polarization state of the incoming light, some special means of achieving highly accurate cross-calibration will be required to reach a verifiable and reliable measurement uncertainty of 0.5%. As shown in the next section, this can be achieved by incorporating an electro-optic polarization modulator into the camera. The most suitable location for this retardance modulator is in the camera's pupil plane.

3. THEORETICAL BACKGROUND

The polarimetric state of light incident on an optical system can be represented by the Stokes vector $\vec{I} = (I, Q, U, V)$, where the component I is the total intensity; Q represents the excess of light at 0° orientation to a specified plane relative to the intensity at 90°; U is the excess of intensity at 45° relative to 135°; and V is the excess of right-handed circular polarization to left-handed circular polarization. DOLP is given by:

$$\mathrm{DOLP} = \frac{\sqrt{(Q^2 + U^2)}}{I} = \sqrt{\left(\frac{Q}{I}\right)^2 + \left(\frac{U}{I}\right)^2} \tag{1}$$

The amount of circular polarization is expected to be on the order of 0.1% of the total intensity, and is ignored in the subsequent discussion. Even though this is small, the requirement to measure linear polarization to 0.5% means that the optical system needs to be designed such that cross-talk of V into Q or U is avoided. In addition, circular polarization introduced by the instrument needs to be minimized, since this causes a loss of efficiency in measuring Q and U.

We assume that under normal (science) operations, the optical system is trimmed to zero retardance, and the focal plane contains one line array overlain by an analyzer at 0°, another line array with an analyzer at 45°, and a third with an analyzer at 90°. The measurements on the three detectors are then given by:

$$I_0 = \frac{1}{2}[I + Q] = \frac{I}{2}\left[1 + \frac{Q}{I}\right]$$
$$I_{45} = \frac{1}{2}[I + U] = \frac{I}{2}\left[1 + \frac{U}{I}\right]$$
$$I_{90} = \frac{1}{2}[I - Q] = \frac{I}{2}\left[1 - \frac{Q}{I}\right] \tag{2}$$

from which the quantities needed to calculate DOLP can be determined by constructing the ratios

$$\frac{I_{90}}{I_0} = \frac{\left[1 - \frac{Q}{I}\right]}{\left[1 + \frac{Q}{I}\right]} \qquad \frac{I_{45}}{I_0} = \frac{\left[1 + \frac{U}{I}\right]}{\left[1 + \frac{Q}{I}\right]} \tag{3}$$

However, if the gains among the different detectors are not accurately cross-calibrated, the values of Q/I and U/I derived from Eq. (3) will lead to errors. Our solution to this problem assumes that a circular retarder is introduced into the optical system, using a birefringent materials in which there is a different refractive index along two orthogonal axes. A circular retarder is a device with its fast axis oriented at 45°, sandwiched between two crossed quarter-wave plates, one with its fast axis at 0° and the other at 90°. Its Muelier matrix is given by:

$$M_{\text{circular retarder}} = \begin{bmatrix} 1 & 0 & 0 & 0 \\ 0 & \cos\delta & \sin\delta & 0 \\ 0 & -\sin\delta & \cos\delta & 0 \\ 0 & 0 & 0 & 1 \end{bmatrix} \tag{1}$$

where δ is the retardance of the birefringent material. Then, the measurements on the three detectors are:

$$I_0 = \frac{1}{2}[I + \cos\delta Q + \sin\delta U]$$
$$I_{45} = \frac{1}{2}[I - \sin\delta Q + \cos\delta U]$$
$$I_{90} = \frac{1}{2}[I - \cos\delta Q - \sin\delta U] \tag{4}$$

which means that with a variable retarder in which $\delta = \delta(t)$ (i.e., the retardance is a function of time), it is possible to modulate the portions of the signals depending on Q and U.

Uniform materials such as glass become birefringent when compressed along one axis. This is commonly referred to as stress-induced birefringence, or the photoelastic effect. By making use of mechanically resonant oscillation, it is possible to construct a variable retarder with a power requirement of only about 1 W. By coupling a piezoelectric transducer to a glass or fused silica bar, a standing sound wave that oscillates at the bar's fundamental frequency is induced. This causes a modulation of the birefringence at a frequency, ω, equal to $c_s/(2L)$, where c_s is the speed of sound in the glass and L is the length of the bar. For bars several cm long the frequency is ~50 kHz. The stress-induced retardance δ for these photoelastic modulators (PEMs) is given by

$$\delta(t) = \delta_0 \sin\omega t \tag{5}$$

where δ_0 is the amplitude of the oscillation. The amplitude δ_0 can be regulated with an electronic feedback circuit.

Because the material out which PEMs are constructed is glass or fused silica, transmittance over a wide spectral range is possible. The principal drawback of PEMs is that they are mechanically delicate. In order to produce a standing sound wave, the oscillating parts can only be held (softly) at a few points. The joint between the piezoelectric transducer and the glass is also susceptible to stress. During launch, it may be necessary to clamp the PEM and then remove that clamp in orbit. Nonetheless, such devices have been demonstrated to achieve polarimetric sensitivities (i.e., precision) of about 3 parts in 10^6 in solar astronomy applications using ground-based telescopes[26].

The required fast electro-optic retardance modulator could in principle be constructed from liquid crystals, and although ferroelectric devices have tuning speeds of 30-250 μsec[25], the chromophores transmit only over limited spectral range, e.g., 400 - 700 nm. Another way of modulating retardance rapidly is to use a mechanically spinning waveplate. However, this will introduce some vibrations into the system. Fabrication tolerances and bearing wear will cause some wobble of the reflected light as well as optical wavefront phase shifts. Although magnetic levitation bearings have non-contacting interfaces, thus avoiding friction and wear, they are bulky and currently not available in the compact sizes needed for our application. Thus, the solid-state construction, high optical quality, and broad spectral transmittance make PEMs very attractive for our purposes.

To understand the implications of using a PEM to assist in cross-calibrating the line arrays represented by Eq. (4), we use the Bessel function expansions of the cosine and sine of a sinusoid[27] and combine Eqs. (4) and (5) to obtain:

$$I_0 = \frac{1}{2}[I + J_0(\delta_0)Q] + \left[\sum_{k=1}^{\infty} J_{2k}(\delta_0)\cos 2k\omega t\right]Q + \left[\sum_{k=0}^{\infty} J_{2k+1}(\delta_0)\sin([2k+1]\omega t)\right]U$$

$$I_{45} = \frac{1}{2}[I + J_0(\delta_0)U] + \left[\sum_{k=1}^{\infty} J_{2k}(\delta_0)\cos 2k\omega t\right]U - \left[\sum_{k=0}^{\infty} J_{2k+1}(\delta_0)\sin([2k+1]\omega t)\right]Q$$

$$I_{90} = \frac{1}{2}[I - J_0(\delta_0)Q] - \left[\sum_{k=1}^{\infty} J_{2k}(\delta_0)\cos \omega t\right]Q - \left[\sum_{k=0}^{\infty} J_{2k+1}(\delta_0)\sin([2k+1]\omega t)\right]U \qquad (6)$$

3.1 Amplitude modulation

The oscillation frequency of the PEM is much higher than the frequency at which the line arrays from a pushbroom imager must be read out (~25 Hz to achieve 250 m spacing between successive lines). Thus, we can use the high frequency retardance modulation provided by the PEM is used as a means to temporally average out the Stokes vector components, in effect operating the PEM as an electro-optic polarization scrambler. During normal science operations the PEM would be turned off. But during intermittent calibration sequences, we can see from Eq. (6) that after a line-array integration time that is long compared to the period of one cycle of the PEM), the time-averaged signals are given by

$$\overline{I_0} = \frac{1}{2}[I + J_0(\delta_0)Q] = \frac{I}{2}\left[1 + J_0(\delta_0)\frac{Q}{I}\right]$$

$$\overline{I_{45}} = \frac{1}{2}[I + J_0(\delta_0)U] = \frac{I}{2}\left[1 + J_0(\delta_0)\frac{U}{I}\right]$$

$$\overline{I_{90}} = \frac{1}{2}[I - J_0(\delta_0)Q] = \frac{I}{2}\left[1 - J_0(\delta_0)\frac{Q}{I}\right] \qquad (7)$$

From Eq. (7) we can see that

$$\frac{\overline{I_{90}}}{\overline{I_0}} = \frac{\left[1 - J_0(\delta_0)\frac{Q}{I}\right]}{\left[1 + J_0(\delta_0)\frac{Q}{I}\right]} \qquad \frac{\overline{I_{45}}}{\overline{I_0}} = \frac{\left[1 + J_0(\delta_0)\frac{U}{I}\right]}{\left[1 + J_0(\delta_0)\frac{Q}{I}\right]} \tag{8}$$

By varying the voltage applied to the PEM it is possible to vary the modulation amplitude δ_0 and therefore the value of the coefficient $J_0(\delta_0)$. The amplitude modulation would have to be slow enough such that the PEM controller can stabilize. Laboratory experimentation shows this adjustment time to be on the order of 400 ms. Since this is much longer than the frame rate, the camera must be viewing a uniform target, which can be a calibration panel or a homogeneous Earth scene such as an ice sheet. By sweeping δ_0 through values where $J_0(\delta_0) = 0$, the arrays can be cross-calibrated because at this value of the amplitude the ratios given in Eq. (8) should be equal to unity. The gains would then be set to provide the same intensity value as a non-polarimetric measurement, obtained by including a line array within the same spectral band but without a polarization analyzer. The beauty of this technique is that the polarization state of the target need not be known. With the PEM turned off, the polarization state of an arbitrary scene can now be reconstructed using Eq. (3).

3.2 Synchronous demodulation

Equation (6) highlights an alternative approach for using a PEM. For a PEM oscillating at 50 kHz, there are 2000 cycles in the 40-ms frame rate. Each cycle therefore lasts 20 μs. Solar astronomers[26,28-30] developed a clever approach in which modulation of the retardance takes place at high frequency using a PEM, and the resulting signal is synchronously demodulated by rapidly shifting charges within a CCD between optically unmasked and masked detector lines at a frequency phase-locked to the PEM resonant frequency. Equation (6) shows that one complete cycle of the PEM can be divided into two sub-intervals in which the measurements are linear sums of I, Q, and U with different coefficients multiplying Q and U. Therefore, by accumulating these individual signals during an integration time, the signals can then be read out at the slower frame rate and processed to reconstruct the Stokes vector. Retrieval of Q and U requires combining the signals from different line arrays. However, since each line array provides relative measurements, this approach is immune to detector gain variations. For our application, where polarimetry up to 1630 nm is required, a CMOS multiplexer, in which charges are alternately shuttled to different caches[31], is required to demodulate the signals. This approach would make it possible to broaden the spectral range since different photoactive materials (e.g., Si in the visible/near-IR and InGaAs in the SWIR) can be integrated with a CMOS multiplexer. Such devices currently do not exist, but we have done preliminary design work suggesting that construction is feasible. The circuit performing the charge summing will need to be low noise to achieve the desired polarization sensitivity. This places severe constraints on the pixel readout circuits. Our calculations show that the circuit must not introduce equivalent noise >10-20 electrons per cycle, implying a fast switching capacitive trans-impedance amplifier (CTIA) technology.

4. CONCLUSIONS

Two approaches making use of a fast retardance modulator to achieve high-accuracy imaging polarimetry have been outlined. Relative to amplitude modulation, synchronous demodulation provides a continuous, rapidly interlaced signal that can better insulate against false polarization from rapid spatial or temporal variation in the observed scene. However, it is significantly more complicated. Making an informed trade-off between complexity and accuracy requires exploring both solutions. We are currently pursuing funding to build laboratory breadboards.

ACKNOWLEDGMENTS

The research of D.J. Diner, S.A. Macenka, T.J. Cunningham, and S. Seshadri is conducted at the Jet Propulsion Laboratory, California Institute of Technology, under contract with the National Aeronautics and Space Administration. We thank N. Raouf of JPL for information regarding the spectral reflectances of mirror coatings.

REFERENCES

[1]Remer, L.A., D. Tanré, Y.J. Kaufman, C. Ichoku, S. Mattoo, R. Levy, D.A. Chu, B.N. Holben, O. Dubovik, A. Smirnov, J.V. Martins, R.R. Li, and Z. Ahmad (2002). Validation of MODIS aerosol retrieval over ocean. *Geophys. Res. Lett.* **29**, 10.1029/2001GL013204.

[2]Chu, D.A., Y.J. Kaufman, C. Ichoku, L.A. Remer, D. Tanré, and B.N. Holben (2002). Validation of MODIS aerosol optical depth retrieval over land. *Geophys. Res. Lett.* **29**, 10.1029/GL013205.

[3]Torres, O., P.K. Bhartia, J.R. Herman, A. Sinyuk, P. Ginoux, and B. Holben (2002). A long-term record of aerosol optical depth from TOMS observations and comparison to AERONET measurements. *J. Atmos. Sci.* **59**, 398-413.

[4]Torres, O., R. Decae, P. Veefkind, and G. de Leeuw (2002). OMI aerosol retrieval algorithm. In *OMI Algorithm Theoretical Basis Document, vol. III*, P. Stammes and R. Noordhoek, eds.

[5]Kahn, R., P. Banerjee, and D. McDonald (2001). The sensitivity of multiangle imaging to natural mixtures of aerosols over ocean. *J. Geophys. Res.* **106**, 18219-18238.

[6]Kalashnikova, O.V., R. Kahn, I.N. Sokolik, and W-H. Li (2004). The ability of multi-angle remote sensing observations to identify and distinguish mineral dust types: Part 1. Optical models and retrievals of optically thick plumes. *J. Geophys. Res.*, in press.

[7]Veefkind, J.P., G. de Leeuw, and P.A. Durkee (1998). Retrieval of aerosol optical depth over land using two-angle view satellite radiometry during TARFOX. *Geophys. Res. Lett.* **25**, 3135-3138.

[8]North, P.R.J., S.A. Briggs, S.E. Plummer, and J.J. Settle (1999). Retrieval of land surface bidirectional reflectance and aerosol opacity from ATSR-2 multi-angle imagery. *IEEE Trans. Geosci. Remote Sens.* **37**, 526-537.

[9]Robles González, C. (2003). Retrieval of aerosol properties using ATSR-2 observations and their interpretation. Ph.D. Thesis, University of Utrecht, Netherlands.

[10]Martonchik, J. V., D.J. Diner, B. Pinty, M.M. Verstraete, R.B. Myneni, Y. Knyazikhin, and H.R. Gordon (1998). Determination of land and ocean reflective, radiative and biophysical properties using multiangle imaging. *IEEE Trans. Geosci. Remote Sens.* **36**, 1266-1281.

[11]Martonchik, J.V., D.J. Diner, K.A. Crean, and M.A. Bull (2002). Regional aerosol retrieval results from MISR. *IEEE Trans. Geosci. Remote Sens.* **40**, 1520-1531.

[12]Moroney, C., R. Davies, and J-P. Muller, Operational retrieval of cloud-top heights using MISR data. IEEE Trans. Geosci. Remote Sens. 40, 15-41, 2002.

[13]Muller, J-P., A. Mandanayake, C. Moroney, R. Davies, D.J. Diner, and S. Paradise (2002). MISR stereoscopic image matchers: Techniques and results. *IEEE Trans. Geosci. Remote Sens.* **40**, 1547.

[14]Zong, J., R. Davies, J-P. Muller, and D.J. Diner (2002). Photogrammetric retrieval of cloud advection and top height from the Multi-angle Imaging SpectroRadiometer (MISR). *Photogramm. Eng. and Remote Sens.* **68**, 821.

[15]Naud C., J-P. Muller, M. Haeffelin, Y. Morille and A. Delaval (2004). Assessment of MISR and MODIS cloud top heights through inter-comparison with a back-scattering lidar at SIRTA. *Geophys. Res. Lett.* **31**, L04114, doi:10.1029/2003GL018976.

[16]Mishchenko, M.I. and L.D. Travis (1997). Satellite retrieval of aerosol properties over the ocean using polarization as well as intensity of reflected sunlight. *J. Geophys. Res.* **102**, 16989-17014.

[17]Cairns, B., L.D. Travis, and E.E. Russell (1999). The Research Scanning Polarimeter: Calibration and ground-based measurements. *Proc. SPIE* **3754**, 186-196.

[18]Chowdhary, J., B. Cairns, M. Mishchenko, and L. Travis (2001). Retrieval of aerosol properties over the ocean using multispectral and multiangle photopolarimetric measurements from the Research Scanning Polarimeter. *Geophys. Res. Lett.* **28**, 243-246.

[19]Chowdhary, J., B. Cairns, and L.D. Travis (2002). Case studies of aerosol retrievals over the ocean from multiangle, multispectral photopolarimetric remote sensing data. *J. Atmos. Sci.* **59**, 383-397.

[20]Deuzé, J.L., P. Goloub, M. Herman, A. Marchand, G. Perry, S. Susana, and D. Tanré (2000). Estimate of the aerosol properties over the ocean with POLDER. *J. Geophys. Res.* **105**, 15329-15346.

[21]Hagolle, O., P. Goloub, P.Y. Deschamps, H. Cosnefroy, X. Briottet, T. Bailleul, J.M. Nicolas, F. Parol, B. Lafrance, and M. Herman (1999). Results of POLDER in-flight calibration. *IEEE Trans. Geosci. Remote Sens.* **37**, 1550-1566.

[22]Ohring, G., B. Wielicki, R. Spencer, W. Emery, and R. Datla (eds.) (2004). Satellite instrument calibration for measuring global climate change. Report from the Nov 12-14, 2002 Workshop, NISTIR 7047, 119pp.

[23]Ramanathan, V., T.S. Bates, J.E. Hansen, D.J. Jacob, Y.J. Kaufman, J.E. Penner, M.J. Prather, S.E. Schwartz, and J.H. Seinfeld (2002). The National Aerosol-Climate Interactions Program (NACIP) white paper. http://www-nacip.ucsd.edu.

[24]Diner, D.J., J.C. Beckert, T.H. Reilly, C.J. Bruegge, J.E. Conel, R.A. Kahn, J.V. Martonchik, T.P. Ackerman, R. Davies, S.A.W. Gerstl, H.R. Gordon, J-P. Muller, R.B. Myneni, P.J. Sellers, B. Pinty, and M. Verstraete (1998). Multi-angle Imaging SpectroRadiometer (MISR) instrument description and experiment overview. *IEEE Trans. Geosci. Rem. Sens.* **36**, 1072-1087.

[25]Boulder Nonlinear Systems (2001). Ferroelectric liquid crystal based polarization filters. http://dev.bouldernonlinear.com/papers/FerroPolarFilters.pdf.

[26]Gandorfer, A.M. and H.P. Povel (1997). First observations with a new imaging polarimeter. *Astron. Astrophys.* **328**, 381-389.

[27]Abramowitz, M. and I.A. Stegun (1965). Handbook of mathematical functions. Dover Publications, Inc., NY.

[28]Stenflo, J.O. and H. Povel (1985). Astronomical polarimeter with 2-D detector arrays. *Appl. Opt.* **24**, 3893-3898.

[29]Povel, H., H. Aebersold, and J.O. Stenflo (1990). Charge-coupled device image sensor as a demodulator in a 2-D polarimeter with a piezoelastic modulator. *Appl. Opt.* **29**, 1186-1190.

[30]Povel, H., C.U. Keller, and I.-A. Yadigaroglu (1994). Two-dimensional polarimeter with a charge-coupled-device image sensor and a piezoelastic modulator. *Appl. Opt.* **33**, 4254-4260.

[31]Keller C.U. (2003). Charge-Caching CMOS Detector for Polarimetry (C3Po). *Proc. SPIE* **5171**.